Verification Study of Sliding and Overset Grid Methods using the Method of Manufactured Solutions on a Wind Turbine flow

Tiago Gomes[*], **Sébastien Lemaire**[† §], **Guilherme Vaz**[‡ † ⋆ ¶], **and Fernando Lau**[*]
[*]Instituto Superior Técnico, Lisboa/Portugal, [†]Maritime Engineering Group, University of Southampton, Southampton/UK, [‡]WavEC, Lisbon/Portugal, [§] MARIN, Wageningen/Netherlands, [⋆]ISMT, Universität Duisburg-Essen, Duisburg/Germany, [¶] blueOASIS, Lisbon/Portugal
tiago.gomes.21@tecnico.ulisboa.pt

1 Introduction

Sliding Grids (SG) and Overset Grids (OG) are two CFD methods for discretizing the domain with several sub-grids, with the potential of: 1) simplifying the mesh generation process; 2) increase their individual quality; 3) improve accuracy of unsteady simulations with moving objects. Their fundamental difference lies on the sub-grid placement, fitted into each other (SG) or overlapped (OG), which ends up impacting the information transfer mechanism that couples them. During the last few years, both methods have been specially useful in many areas, including the simulation of offshore wind turbines, where a Sliding Grid might be used to accommodate the motion of the rotor and an Overset Grid to capture the overall movement of the platform with the ocean waves (Tran and Kim, 2018). However, very few studies exist comparing SG with OG, despite their versatility and interchangeability in various situations. Even within the available literature, as (Francois et al., 2011), they mostly focus on practical test cases, with no Code Verification (Eça and Hoekstra, 2013) performed. Therefore, a detailed analysis is necessary, where the flow analytical solution is known, so that discretization errors can be evaluated in isolation. For that an inedit wind turbine flow manufactured solution is designed and used, taking advantage of the Method of Manufactured Solutions (Roache, 2019) to produce an arbitrarily complex flow with a known analytical solution. With it, Code Verification can be performed, to assess and compare the impact of SG and OG in typical wind turbine flow conditions. Based on this work, some more light can be shed on possible improvements and good practices for industrial uses, potentially extendable to other CFD solvers with similar capabilities.

2 ReFRESCO

ReFRESCO (Vaz et al., 2009) is a CFD solver based on a finite-volume discretization with cell-centered collocated variables and unstructured grids, capable of handling hanging nodes. It solves the unsteady, multi-phase and incompressible RANS equations, in addition to turbulence models and volume-fraction transport equations for each phase. Moreover, it has the capability to simulate moving objects through the use of Sliding Grids and more recently the Overset Grids method (Lemaire et al., 2021). These methods depend on the interpolation schemes implemented, with a considerable number of options available in the solver. Some of them include Inverse Distance (1st order), Nearest Cell Gradient (2nd order) and Least Squares (n-th order with a $n-1$th degree polynomial) (Lemaire et al., 2021).

3 Sliding Grids Method

The Sliding Grids method uses several sub-grids to discretize the domain (Rai, 1985). Despite being individually generated, they have a certain degree of dependence, since they need to fit into each other to cover the entire domain. Therefore, the sub-grids communicate between each other through the interfaces, which might slide relative to one another in the case they are animated. Considering this, they are inherently limited to simple movements, including unidirectional translation or rotation over cylindrical or conical surfaces of revolution.

A key aspect of the implementation of this method is the information transfer between each sub-grid through the interface. Several methods exist in the literature, but in ReFRESCO the one implemented is based on Halo Cells (Ramírez et al., 2015). In the Halo Cell method the new cell center is projected from a given parent boundary cell at the interface to the other contiguous sub-grid. The properties of the flow at the halo cell center are interpolated from a stencil of surrounding cells in the sub-grid to which it was projected to, based on the selected interpolation scheme. These will act as Dirichlet boundary conditions,

closing the respective system of equations and coupling the sub-grids. In ReFRESCO the halo cells are determined on-the-fly, being by default projected over the line connecting the parent cell center and the respective face center. Therefore, no eccentricity exists between both. Moreover, the halo cell is defined to have the same size as the parent cell.

4 Overset Grids Method

The Overset Grids method (Benek et al., 1986) also uses several sub-grids to discretize the domain. However, since they are overlapped, they don't need to fit into each other, potentially easing the grid generation process and allowing virtually any type of movement because of that same characteristic. Nevertheless, they are known to be numerically more expensive and also more complex to implement than the Sliding Grids method (Francois et al., 2011).

This method uses the Domain Connectivity Information (DCI), which assigns to each cell in the domain one of three possible status: *In*, *Fringe* or *Hole* Cell. *In* Cells are regular, active cells in the domain. *Hole* Cells are the ones that are ignored by the solver, since they are substituted by cells of other sub-grid that is overlapping that region or because they are just outside the domain. Finally, *Fringe* cells are placed in between the two other types of cells, receiving the interpolated information and coupling the different sub-grids.

5 Wind Turbine MMS Test Case

The wind turbine flow solution was created based on the Method of Manufactured Solutions (MMS). A CFD simulation of an Actuator Disk was used as reference to model the velocity and pressure fields, which in turn had as inputs the reference operating conditions of the NREL 5MW (Jonkman et al., 2009) wind turbine: free-stream flow velocity, V_0, of 11.4 m/s, rotor angular speed, ω, of 1.2698 rad/s and respective values of thrust and torque. The z axis represents the flow direction, perpendicular to the rotor disk.

After extensive testing, Equation (1) was obtained, providing a V_z field with reasonable features and a power net flux, P_{net} , over the selected domain of around 5.008 MW (harvested). This process included tunning the values of the blending functions in the axial and radial directions, Equations (3) and (4), respectively, where R_a is the radius of the wind turbine, 63 meters. In order to respect the continuity equation, the integral of Equation (2) was solved using the algebraic toolbox Sympy, obtaining the radial velocity distribution V_r. While the tangential component V_θ did not contribute to mass conservation, it was not considered to simplify the solution process.

$$\begin{aligned} V_z(r,z) = V_0 &- 0.2715 \cdot V_0 \cdot \gamma_z(z, 0.7, 4.0) \cdot \gamma_r(r, 1.2) \\ &+ 0.2000 \cdot V_0 \cdot \gamma_z(z, 0.7, 4.0) \cdot \gamma_r(r, 2.5) \\ &- 0.1000 \cdot V_0 \cdot \gamma_z(z, -2.0, 1.0) \cdot \gamma_r(r, 3.0) \end{aligned} \tag{1}$$

$$V_r = \frac{1}{r}\left(\int_0^r -r\frac{\partial V_z}{\partial z}dr\right) \tag{2}$$

$$\gamma_z(z, a, b) = \frac{1}{1 + e^{(\frac{z}{R_a}+a)\cdot b}} \tag{3}$$

$$\gamma_r(r, c) = e^{\left(-c\cdot\frac{r}{R_a}\right)^2} \tag{4}$$

As for the pressure field, p, the strategy adopted was based on the Bernoulli's Principle, presented in Equation (6). Assuming that the total pressure H is constant along a streamline, a reasonable approximation given the flow characteristics, all flow regions will have the same value as the free-stream flow, H_0, with p_0 equal to 0 Pa. The only exception will be in the wake, since energy was extracted from the flow by the turbine. Based on dimensional analysis, Equation (5) was obtained to estimate that drop in total pressure, obtaining H_{wake} with previously known quantities. Afterwards, the two total pressure values obtained, H_0 and H_{wake}, were blended in a similar fashion to V_z, allowing for a pressure field equation to be obtained through Equation (6).

$$H_{wake} = H_0 + \frac{P_{net}}{Q_{disk}} \tag{5}$$

$$p(r,z) = H(r,z) - \frac{1}{2}\rho V(r,z)^2 \tag{6}$$

$$H(r,z) = (H_0 \cdot (1 - \gamma_z(z, 0.0, 4.0)) + H_{wake} \cdot \gamma_z(z, 0.0, 4.0)) \cdot \gamma_r(r, 1.2)) + H_0 \cdot (1 - \gamma_r(r, 1.2)) \tag{7}$$

Having created a set of equations describing the velocity and pressure fields in the domain, pyMMS

(Lemaire, 2021) was used to obtain the source terms that forced them to become the exact solutions of the Navier-Stokes equations. These source terms are in turn provided to the flow solver, which eventually outputs a simulation with errors that can be easily assessed by comparison with the known analytical solution provided initially - thefore enabling Code Verification. A slice of the obtained velocity and pressure fields are presented in Figure 1.

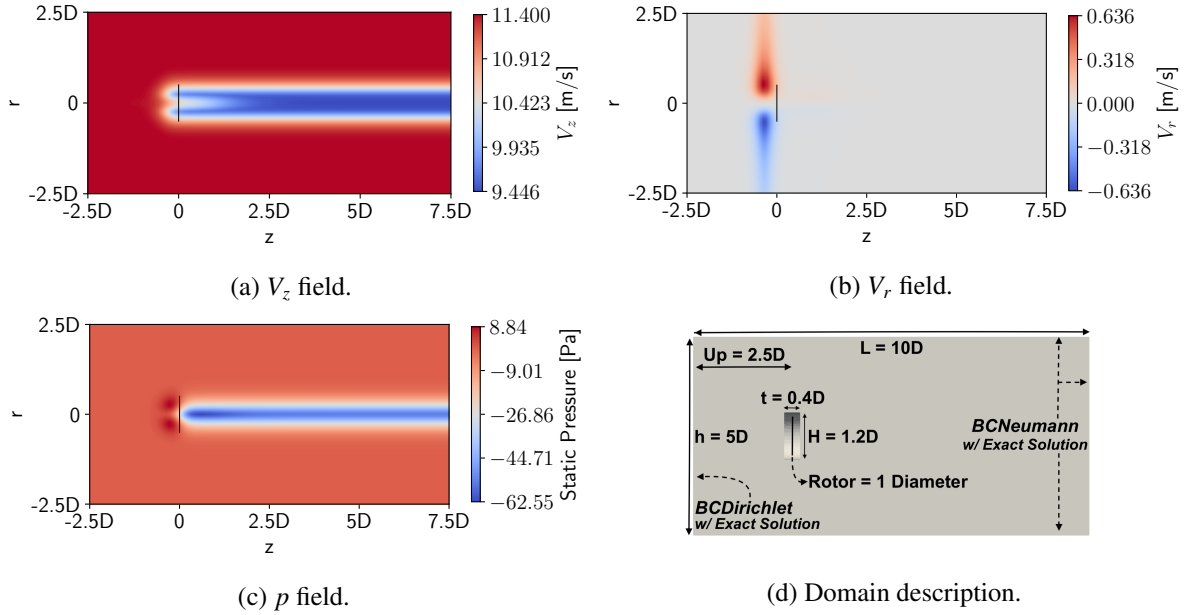

(a) V_z field.

(b) V_r field.

(c) p field.

(d) Domain description.

Fig. 1: Exact solution fields of Wind Turbine MMS, based on Actuator Disk solution with NREL 5MW characteristics. Slice over rz plane, in cylindrical coordinates.

While solution realism is not essential to a MMS (Roache, 2019), it was still sought during the creation process. Nevertheless, issues with the stability of MMS that did not respect continuity severely limited the flow features that could be recreated. Therefore the present MMS represents a compromise, which can have some critics established: (1) the wake has no swirl, $V_\theta = 0$; (2) the wake has no expansion; (3) the flow starts decelerating too early upstream of the turbine, which leads to premature radial velocity component. In the end the authors acknowledge the limitations of the current MMS, but hope to further improve it in the future after identifying and solving the stability issues stated. Yet, it is considered that the current version is already suitable to perform Code Verification.

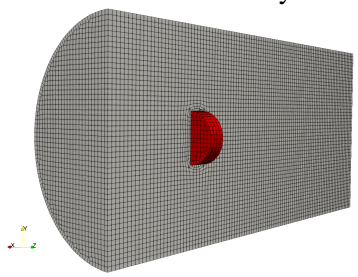

Fig. 2: Typical SG grid setup. Slice over yz (or rz) plane of Hole subgrid (gray), fitted with Rotor subgrid (red). G1 refinement. Cylinder grid is identical to Hole, but without space to fit Rotor.

Grid	Refin. (h_i)	Size	Cell Count (N_i)		
		Cylinder	Cylinder	Rotor	Hole
G1	2.49	100 x 50 x 50	203 600	512	204 144
G2	1.66	150 x 75 x 75	682 350	1680	682 839
G3	1.25	200 x 100 x 100	1 604 000	3840	1 603 700
G4	1.00	250 x 125 x 125	3 125 250	7520	3 123 035

Table 1: Sub-grid refinements description. Baseline: Cylinder grid only. Sliding Grids: Hole mesh fitted with Rotor grid. Overset Grids: Cylinder and Rotor grids overlapped.

To discretize the domain, three main types of grids had to be created. The first is a simple, Cylinder grid with mostly cubic cells, which is used as a benchmark, since it is a single mesh. This grid will also

be used in OG, together with a second sub-grid, Rotor, overlapped in the region of the wind turbine, which can rotate. Finally, for the SG, the Rotor sub-grid will also be used, but the Cylinder one is substituted with another that has a hole in the middle, so that they can fit into each other. All grids are unstructured, created using Hexpress, aiming at geometric similarity through all refinements, resulting in a set of systematically refined grids necessary to perform Code Verification. Moreover, they do not have hanging nodes. Their characteristics are presented in Figure 2 and Table 1.

The boundary conditions (BC) were defined as follows: a Dirichlet BC for the inlet and a Neumann BC for the other exterior surfaces, all based on the analytical solution of the MMS. Regarding the adopted numerical setup, for the discretization of the convection fluxes a 2nd order, limited, QUICK scheme was selected. For the time discretization the 2nd order Implicit Three Time Level is used, with a default angular rotation per time step of 8 degrees (maximum CFL is 0.25 in grid G4, with a time step of 0.11 s). The iterative residuals are reduced up until all L_∞ norms are below 10^{-6} at each time step, which yield iterative errors negligible for all flow quantities after an iterative study was performed. Finally, for both SG and OG the default interpolation scheme used is the Least Squares with a second degree polynomial function, which is a third order accurate scheme (LS3).

6 Results

6.1 Baseline

The first simulation used a single grid for the entirety of the domain, serving as a benchmark when SG and OG methods are introduced. Overall, at least second order of accuracy was obtained for pressure and radial velocity components (V_x and V_y). However, for the axial velocity, V_z, reduced order of accuracy occured ($p = 1.37$). Due to a yet unknown source, high errors concentrated at the outlet of the domain, degrading the overall velocity error order. Hence, focus will be given to the L_2 error norms throughout this work to assess the impact of the SG and OG, instead of L_∞, which are dominated by these outlet errors. Nevertheless, no significant impact is expected on the conclusions of the present paper.

6.2 Time Step

One of the parameters tested was the influence of the time step. Assuming that the rotor has a fixed angular speed during operation ($\omega = 1.2698$ rad/s), the time step is determined in order for the rotor to advance a pre-determined amount of degrees. The values tested ranged from 6 to 24 degrees per time step (6 to 24 $^\circ/\Delta t$). The movement of the rotor leads to unsteadiness of the results, which need to be averaged. To quantify the respective statistical uncertainty the TST method is used (Brouwer et al., 2015), as implemented in the software pyTST (Lemaire and Klapwijk, 2021). In this particular case that quantity was always kept at least two orders of magnitude lower than the obtained mean by taking into account the last four rotations of the rotor in the simulation.

The grid refinement plots of V_x error for different time steps are presented in Figures 3a and 3b, for SG and OG, respectively. Based on the methodology of Code Verification (Eça and Hoekstra, 2013), a linear regression was used to estimate the order of convergence, p, presented in Figure 3c.

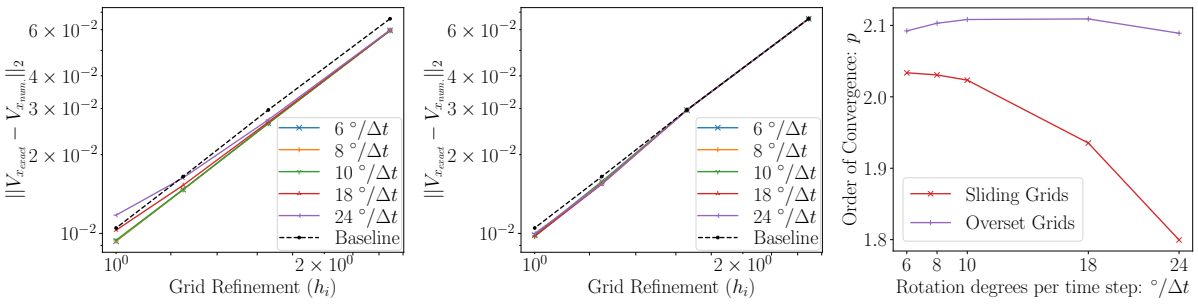

(a) V_x error (L_2 norm). Sliding Grids. (b) V_x error (L_2 norm). Overset Grids. (c) Order of Convergence, p.

Fig. 3: Time Step sensitivity study: 6 to 24 degrees of rotation per timestep. Analysed quantity: V_x error.

It can be concluded that the order of convergence of V_x is degraged with coarser time steps when

SG are used, whereas OG appears to be more robust in preserving it. Analyzing the error curves, neither of the methods seem to be introducing a significant source of error. In fact, the slight error reduction perceived in some grids when compared to the Baseline case is likely related to the reduced amount of cells of the latter. Moreover, the OG results match the Baseline for G1 and G2: this is due to the lack of Fringe cells in the domain, given that these meshes are too coarse, therefore errors from the rotor are not transmitted to the rest of the domain. Besides, this consideration is behind a slight overprediction of the order of convergence in Figure 3c for OG.

Overall, as finer grids are used with SG, the convergence decreases if coarse time steps are adopted. On the other hand, OG is pratically not influenced by that. Regarding other flow quantities, V_y presented the exact same results, since the flow is axyssimetric. As for pressure and axial velocity, no significant differences were found in both methods.

6.3 Interpolation Scheme

The other parameter tested was related to the interpolation schemes to couple the sub-grids. The default time step is constant, $8\ ^\circ/\Delta t$. Besides the Least Squares with a second order polynomial (LS3), the default scheme used until this point, Nearest Cell Gradient (NCG2) and Inverse Distance (ID1) were also tested. Note that the algorithm in the acronym denotes the accuracy order of the method. In Figure 6 the error distribution of V_z in the rotor region are presented for the three interpolation schemes (ID1, NCG2 and LS3) for both SG and OG methods. It can be assessed that ID1, a first order method, is introducing

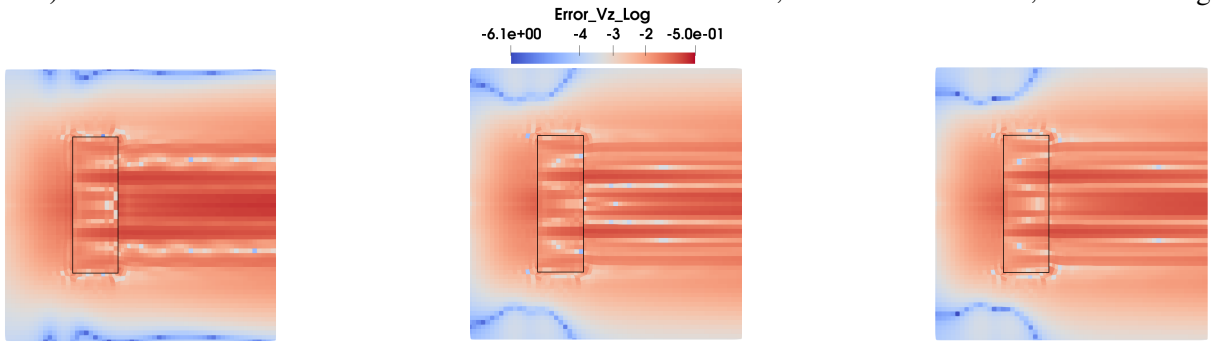

(a) ID1 - SG. (b) NCG2 - SG. (c) LS3 - SG.

(d) ID1 - OG. (e) NCG2 - OG. (f) LS3 - OG.

Fig. 4: Error distribution of axial velocity, V_z, nearby the rotor region in log scale. Slice over yz plane. Black line encloses rotor region. Top row: Sliding Grids. Bottom row: Overset Grids.

the highest amount of errors. These are in turn convected downstream, since this flow is convection dominated. On the other hand, only slight differences can be perceived between the error distribution of NCG2 and LS3, with the second order method introducing a less smooth distribution. Comparing the results between SG and OG, the error wake is wider in the first method, since SG always transfers information at the interface. As for OG that transfer depends on the Fringe cells locations, which in this case are more packed inside the rotor region.

Mass conservation was also investigated, since both SG and OG do not respect it in the intergrid communication process. It is quantified with the absolute value of the sum of mass fluxes going in and out of the domain, with the respective history over the last four rotations presented in Figure 5.

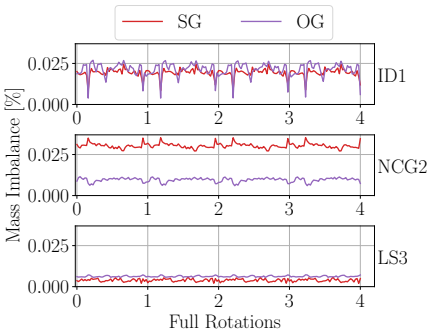

Fig. 5: Mass Imbalance over last rotations: percentage of mass flow rate through the rotor. Grid G4 with different interpolation schemes.

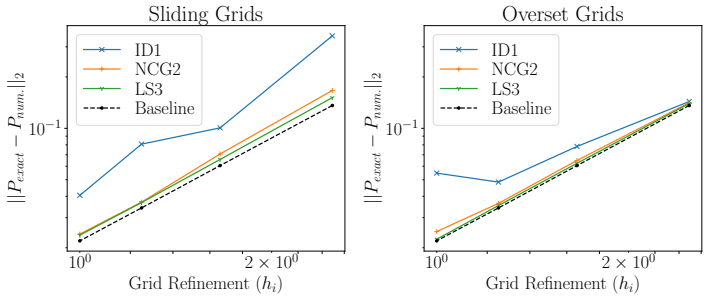

Fig. 6: Pressure errors (L_2 norm) with grid refinement and different interpolation schemes.

Overall, the mass imbalance introduced is minimal: less than 0.03%. Also, the difference between that value using either SG and OG is also small, except for NCG2. However, it is important to point out the differences between each interpolation scheme. While no clear trend exists regarding higher order schemes and lower mean value of mass imbalance (*vide* ID1 vs. NCG2 with SG), the same cannot be said concerning the oscillations. In fact, the higher the order of accuracy of the scheme, the smaller the oscillations. Bear in mind that oscillations in mass imbalance translate into pressure fluctuations, since both quantities are coupled in the pressure correction equation in incompressible flows. These pressure fluctuations are in turn translated to force oscilations. Therefore, while a constant mass imbalance might not be important to the solution accuracy, having oscillations in pressure might have a negative impact when accoustics or forces are under analysis. In fact, Figure 6 reflects this same consideration: ID1 has the highest pressure errors, with SG not being in the assymptotic range and OG errors stagnating in finer grids. On the other hand, NCG2 and LS3 are able to have similar error tends in terms of pressure for both methods, keeping it low and preserving the order of convergence.

Acknowledgements

This project has received funding from the EPSRC Centre for Doctoral Training in Next Generation Computational Modelling (EP/L015382/1) at the University of Southampton including financial support from MARIN. The authors acknowledge the use of WavEC resources and facilities for this work.

References

Benek, J., Steger, J., Dougherty, F., and Buning, P. (1986). Chimera: A Grid-Embedding Technique. *Technical Report AEDC-TR-85-64*.

Brouwer, J., Tukker, J., and van Rijsbergen, M. (2015). Uncertainty analysis and stationarity test of finite length time series signals. In *4th International Conference on Advanced Model Measurement Technologies for the Maritime Industry*.

Eça, L. and Hoekstra, M. (2013). Verification and validation for marine applications of CFD. *International Shipbuilding Progress*, 60(1-4):107–141.

Francois, B., Costes, M., and Dufour, G. (2011). Comparison of Chimera and Sliding Mesh Techniques for Unsteady Simulations of Counter Rotating Open-Rotors. In *20th International Society for Airbreathing Engines Conference*.

Jonkman, J., Butterfield, S., Musial, W., and Scott, G. (2009). Definition of a 5-MW Reference Wind Turbine for Offshore System Development. Technical Report NREL/TP-500-38060, 947422.

Lemaire, S. (2021). pyMMS. DOI: 10.5281/zenodo.4428181.

Lemaire, S. and Klapwijk, M. (2021). pyTST. DOI: 10.5281/zenodo.4428158.

Lemaire, S., Vaz, G., Deij - van Rijswijk, M., and Turnock, S. R. (2021). On the Accuracy, Robustness and Performance of High Order Interpolation Schemes for the Overset Method on Unstructured Grids. *International Journal for Numerical Methods in Fluids*. DOI: 10.1002/fld.5050.

Rai, M. (1985). An Implicit, Conservative, Zonal-Boundary Scheme for Euler Equation Calculations. *NASA Contractor Report 3865 - Ames Research Center*.

Ramírez, L., Foulquié, C., Nogueira, X., Khelladi, S., Chassaing, J. C., and Colominas, I. (2015). New high-resolution-preserving sliding mesh techniques for higher-order finite volume schemes. *Computers and Fluids*, 118:114–130.

Roache, P. J. (2019). The Method of Manufactured Solutions for Code Verification. In Beisbart, C. and Saam, N. J., editors, *Computer Simulation Validation: Fundamental Concepts, Methodological Frameworks, and Philosophical Perspectives*, chapter 12, pages 295–318. Springer International Publishing, Cham.

Tran, T. T. and Kim, D. H. (2018). A CFD study of coupled aerodynamic-hydrodynamic loads on a semisubmersible floating offshore wind turbine. *Wind Energy*, 21(1):70–85.

Vaz, G., Jaouen, F., and Hoekstra, M. (2009). Free-Surface Viscous Flow Computations: Validation of URANS Code FreSCo. In *Proceedings of the ASME 2009 28th International Conference on Ocean, Offshore and Arctic Engineering*, Volume 5: Polar and Arctic Sciences and Technology; CFD and VIV, pages 425–437.